Japanese Journal of Applied Physics

REGULAR PAPER

Effect of ion-beam bombardment on microstructural and magnetic properties of $Ni_{80}Fe_{20}$/α-Fe_2O_3 thin films

To cite this article: Chao Zheng *et al* 2014 *Jpn. J. Appl. Phys.* **53** 06JB03

Japanese Journal of Applied Physics **53**, 06JB03 (2014) **REGULAR PAPER**
http://dx.doi.org/10.7567/JJAP.53.06JB03

Effect of ion-beam bombardment on microstructural and magnetic properties of $Ni_{80}Fe_{20}/\alpha$-Fe_2O_3 thin films

Chao Zheng[1], Tien-Chi Lan[2], Chin Shueh[2], Ryan D. Desautels[3], Johan van Lierop[3]*, Ko-Wei Lin[2]*, and Philip W. T. Pong[1]*

[1]*Department of Electrical and Electronic Engineering, The University of Hong Kong, Hong Kong*
[2]*Department of Materials Science and Engineering, National Chung Hsing University, Taichung 402, Taiwan*
[3]*Department of Physics and Astronomy, University of Manitoba, Winnipeg, MB, R3T 2N2, Canada*
E-mail: kwlin@dragon.nchu.edu.tw; johan@physics.umanitoba.ca; ppong@eee.hku.hk

Received November 30, 2013; accepted February 28, 2014; published online May 23, 2014

Ion-beam bombardment has been established as an effective way to tune the microstructure and thus modify the magnetic anisotropy of thin film materials, leading to certain remarkable magnetic properties. In this work, we investigated a $Ni_{80}Fe_{20}/\alpha$-Fe_2O_3 bilayer deposited with a dual ion-beam deposition technique. Low-energy argon ion-beam bombardment during the α-Fe_2O_3 deposition led to a decline of crystallinity and interfacial roughness of the bilayer, whereas the grain size distribution remained essentially unchanged. At low temperature, the coercivity exhibited a pronounced decrease after the bombardment, indicating that the effective uniaxial anisotropy in the ferromagnetic layer was dramatically reduced. Such reduction in uniaxial anisotropy was likely attributed to the irreversible transition in the α-Fe_2O_3 grains caused by the ion-beam bombardment, which subsequently modified the anisotropy in the $Ni_{80}Fe_{20}$ layer. The bombarded bilayer also exhibited a larger ΔM_{FC-ZFC} compared to the un-bombarded bilayer, which indicated a stronger exchange coupling between the ferromagnetic layer and the antiferromagnetic layer.

1. Introduction

Iron (Fe) and its oxides have been extensively investigated due to their unique properties that can be applied in various areas, such as energy storage,[1,2] nanotechnology,[3–6] and biomedicine.[7–9] As one of the iron oxides, hematite (α-Fe_2O_3) has drawn much attention because of its remarkable magnetic properties. α-Fe_2O_3 appears to be ferrimagnetic below its Néel temperature ($T_N = 948$ K in the bulk[10]) with a small moment that is a result of spin canting[11] arising from the competition between the different superexchange paths of the octahedral (A-site) and tetrahedral (B-site) Fe-ion sublattices, i.e., ferromagnetic or antiferromagnetic A–A, A–B, and B–B interactions. A reorganization of the antiferromagnetic magnetic structure in α-Fe_2O_3 occurs at ~260 K, the Morin transition temperature (T_M).[12] The moments reorder from perpendicular to parallel to the c-axis,[13] accompanied by the disappearance of the net magnetization.

Several studies on α-Fe_2O_3 nanomaterials reveal that the T_M of such materials can be significantly altered (or suppressed entirely) by adjusting the nanoscale particle sizes,[14] geometry[15] and strain.[16] A suppression of the Morin transition due to decreased grain sizes was also reported in recent research on a $Ni_{80}Fe_{20}/\alpha$-Fe_2O_3 bilayer.[13] However, the effects of the altered grain size and temperature-related anisotropy on the magnetic properties of these bilayers are still not fully understood.

As a surface conditioning technique, ion-beam bombardment has been known as an effective method to tune the microstructure and thus modify the magnetic properties of thin films, which may also provide some clues about the finite-size effect on the magnetic anisotropy in both ferromagnetic and antiferromagnetic layers. In this work, different End–Hall voltages (V_{EH}) of the ion gun were applied to tune the ion-beam bombardment energy. We studied $Ni_{80}Fe_{20}/\alpha$-Fe_2O_3 bilayers, either plain (un-bombarded) with $V_{EH} = 0$ and the α-Fe_2O_3 layer bombarded with $V_{EH} = 70$ V Ar-ions. The influence of the ion-beam bombardment on the coercivity and exchange bias[17] of the thin films was also investigated.

2. Experimental methods

$Ni_{80}Fe_{20}/\alpha$-Fe_2O_3 bilayers were deposited on amorphous SiO_2 substrates using a dual-ion-beam sputtering deposition technique.[18,19] A Kaufman ion source (800 V, 7.5 mA) was used to bombard a commercial Fe target with 3 cm^3/min Ar and an End–Hall ion source was used to bombard the SiO_2 substrate with a mixture of 42% O_2/Ar to oxidize Fe into α-Fe_2O_3 in situ.[13] The End–Hall ion source with 70 V was then used to in situ bombard the α-Fe_2O_3 layer before depositing the $Ni_{80}Fe_{20}$ layer. This bombardment process lasted for five minutes. After that, the Kaufman ion source was used to focus an argon ion beam onto a commercial $Ni_{80}Fe_{20}$ (at. %) target surface in order to deposit the $Ni_{80}Fe_{20}$ layer. Un-bombarded bilayers were made the same way except without the ion bombardment on the α-Fe_2O_3 layer. The microstructure of the bilayer was analyzed with a transmission electron microscope (TEM; JEOL JEM-2010) at 200 kV. The composition of the bombarded bilayer was characterized by X-ray photoelectron spectroscopy (XPS; PHI 5000 Versa Probe). The surface roughness measurement of the α-Fe_2O_3 layer was performed with an atomic force microscope (AFM; NTMDT Solver Pro-M). A Quantum Design magnetic property measurement system (MPMS) was used to measure the magnetic hysteresis loops at 10 K (the bilayers were in-plane field-cooled in 20 kOe from 298 to 10 K), and the temperature dependence of the zero field-cooled (ZFC) and field-cooled (FC) in 100 Oe DC susceptibility. Room temperature (298 K) and 160 K hysteresis loop measurements were performed using a Quantum Design vibrating sample magnetometer (VSM).

3. Results and discussion

3.1 Structural properties

The bombardment effect of the argon ion beam on the $Ni_{80}Fe_{20}/\alpha$-Fe_2O_3 bilayers was characterized by TEM, shown in Fig. 1. A smooth interface (i.e., interfacial roughness <2 nm) was observed in a bombarded $Ni_{80}Fe_{20}$ (~14 nm)/α-Fe_2O_3 (~18 nm) bilayer ($V_{EH} = 70$ V), similar to that of an un-bombarded bilayer ($V_{EH} = 0$ V) reported in Ref. 13.

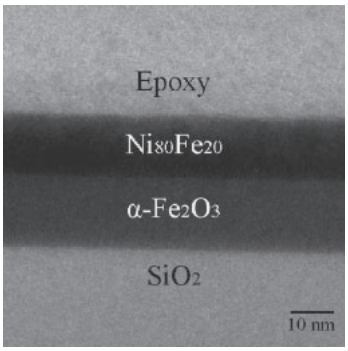

Fig. 1. Cross-sectional TEM image for bombarded [$Ni_{80}Fe_{20}/\alpha$-Fe_2O_3] bilayer.

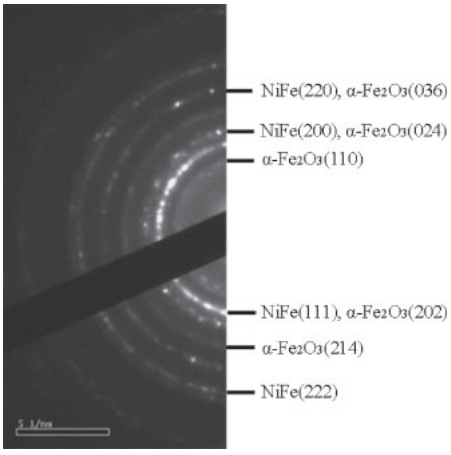

(a)

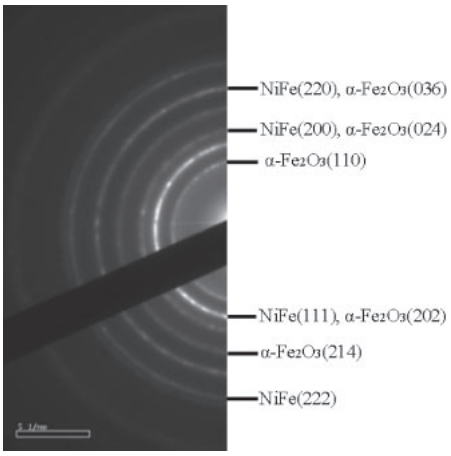

(b)

Fig. 2. Electron diffraction patterns for the un-bombarded (a) and bombarded (b) [$Ni_{80}Fe_{20}/\alpha$-Fe_2O_3] bilayers.

Figures 2(a) and 2(b) are the electron diffraction patterns of the bilayers, which reveal that both the un-bombarded and bombarded bilayers consist of fcc $Ni_{80}Fe_{20}$ and hcp α-Fe_2O_3 crystallites. Specifically, the diffraction rings assigned to (111), (200), and (220) reflections show that the $Ni_{80}Fe_{20}$ layer exhibits a fcc crystalline structure while those assigned to (110), (202), (024), (214), and (036) reflections are from the hcp crystalline structure of the α-Fe_2O_3 layer. The lattice constants for $Ni_{80}Fe_{20}$ ($a \sim 3.51$ Å) and α-Fe_2O_3 ($a \sim 5.16$ Å, $c \sim 13.68$ Å) crystallites derived from the patterns were as expected for the two layers.[20,21] Furthermore, the rings became slightly broader and diffuse in the bombarded bilayer, indicating a decrease of crystallinity in both layers. The decreased crystallinity in the α-Fe_2O_3 caused by the bombardment subsequently affected the crystallization process in the $Ni_{80}Fe_{20}$ layer. More defects were formed on the bombarded α-Fe_2O_3 surface, which were developed during the crystal growth in the $Ni_{80}Fe_{20}$ layer and thus lowered the crystallinity of $Ni_{80}Fe_{20}$. Figure 3 shows the bright- and dark-field TEM images of the α-Fe_2O_3 surfaces without and with bombardment, while Fig. 4 shows the corresponding histograms of the grain size distribution. The values of the grain size for the un-bombarded layer and the bombarded layer ranged from 4 to 16 nm and 4 to 12 nm, respectively. The average grain size (~8 nm) however was not affected by the bombardment.

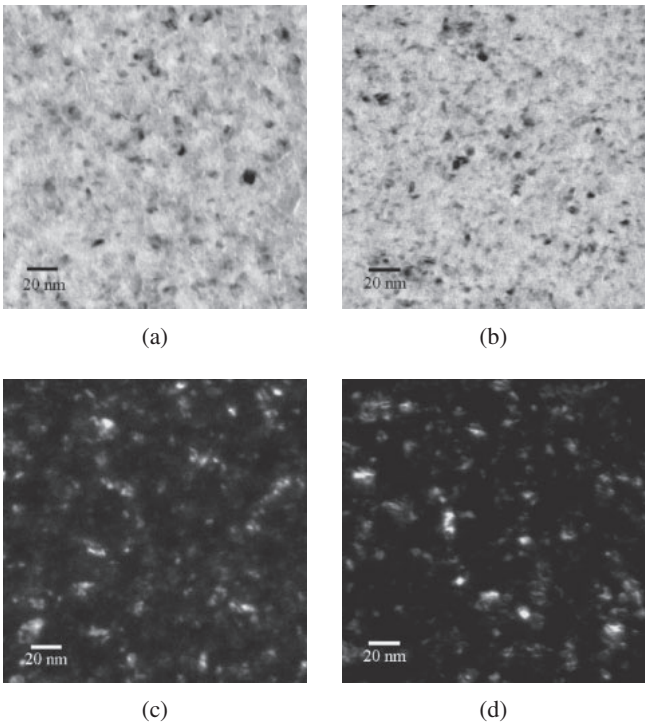

(a) (b)

(c) (d)

Fig. 3. Bright-field and dark-field TEM images of the α-Fe_2O_3 surfaces of the un-bombarded (a, c) and bombarded (b, d) [$Ni_{80}Fe_{20}/\alpha$-Fe_2O_3] bilayers.

The $Ni_{80}Fe_{20}/\alpha$-Fe_2O_3 bilayers' interfacial roughness was characterized by AFM measurement of the α-Fe_2O_3 surface before capping with the $Ni_{80}Fe_{20}$ layer. As shown in Fig. 5, the rms roughness over an $8 \times 8\,\mu m^2$ region of the bilayer was found to decrease from ~2.0 to ~0.8 nm with the $V_{EH} = 70$ V ion-beam bombardment, which indicated a smoother surface in the bombarded bilayer.[22] The wavy surface shown in Fig. 5(b) was likely due to the bumps on the substrate.

Compositional analysis was conducted for the bombarded bilayer. Figures 6(a) and 6(b) show the XPS peaks of Ni 2p, Fe 2p for the $Ni_{80}Fe_{20}$ layer. The Ni 2p spectrum in Fig. 6(a) exhibits two distinct peaks, one at ~852.6 eV attributable to the Ni $2p_{3/2}$ transition while the other at ~869.6 eV attributable to the Ni $2p_{1/2}$ transition.[23] In Fig. 6(b), the Fe 2p spectrum shows two peaks at ~707 and ~719.8 eV corresponding to the Fe $2p_{3/2}$ transition and the Fe $2p_{1/2}$ transition,[23] respectively. It also shows another broad peak at

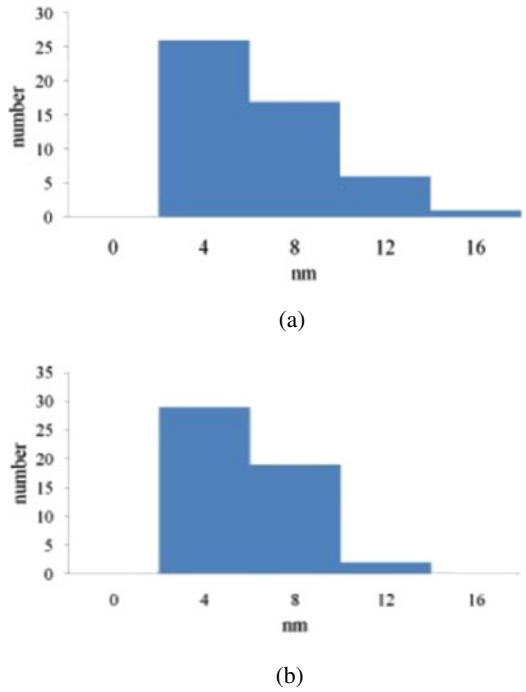

Fig. 4. (Color online) Histograms of the grain size distribution for the un-bombarded (a) and bombarded (b) [$Ni_{80}Fe_{20}$/α-Fe_2O_3] bilayers.

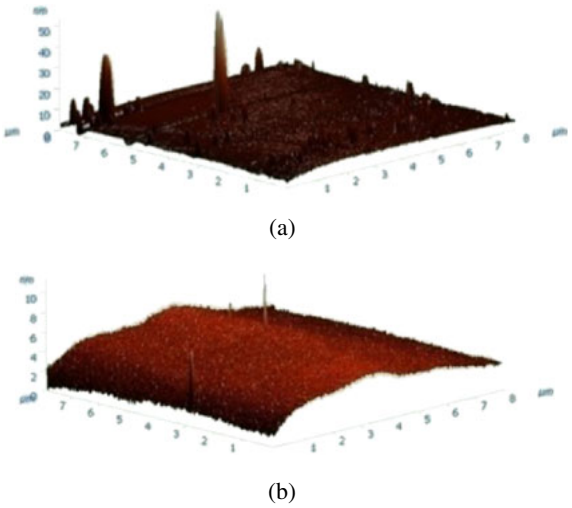

Fig. 5. (Color online) AFM images for the un-bombarded (a) and bombarded (b) [$Ni_{80}Fe_{20}$/α-Fe_2O_3] bilayers.

~712 eV, which is attributed to the Fe $2p_{3/2}$ transition in the Fe_2O_3 phase.[24] This implies a weak intermixing between the $Ni_{80}Fe_{20}$ layer and the α-Fe_2O_3 layer. The O 1s and Fe 2p spectra for the α-Fe_2O_3 layer are displayed in Fig. 7. Figure 7(a) shows the peak of O 1s at ~530.3 eV while Fig. 7(b) shows two peaks at ~709.8 and ~723 eV due to the Fe $2p_{3/2}$ transition and the Fe $2p_{1/2}$ transition,[23] respectively. The depth profile analysis of the bilayer is shown in Fig. 8. The composition of the $Ni_{80}Fe_{20}$ layer is roughly 80 at. % Ni and 20 at. % Fe, in excellent agreement with the target's stoichiometry. On the other hand, the composition of the α-Fe_2O_3 layer is roughly 73 at. % O and 27 at. % Fe. The excess oxygen was attributable to the introduction of O_2 during the bombardment treatment. XPS depth profiling also shows that

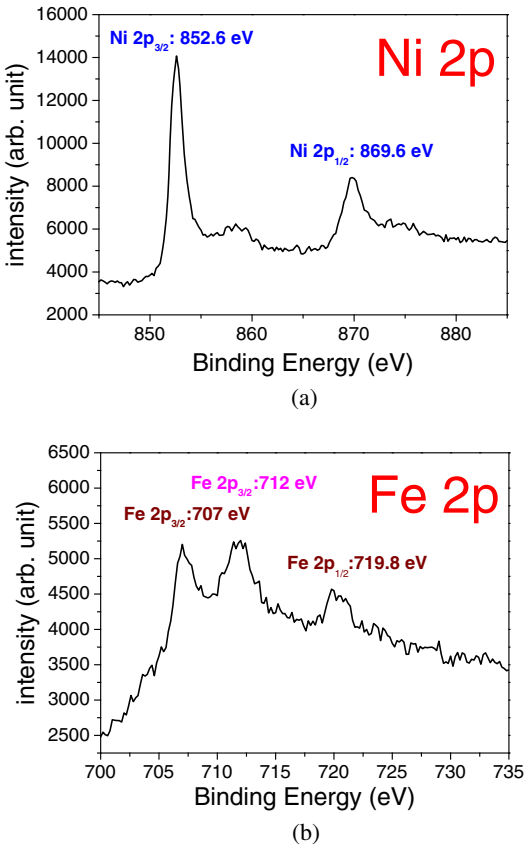

Fig. 6. (Color online) XPS peaks of Ni 2p (a), Fe 2p (b) for the $Ni_{80}Fe_{20}$ layer.

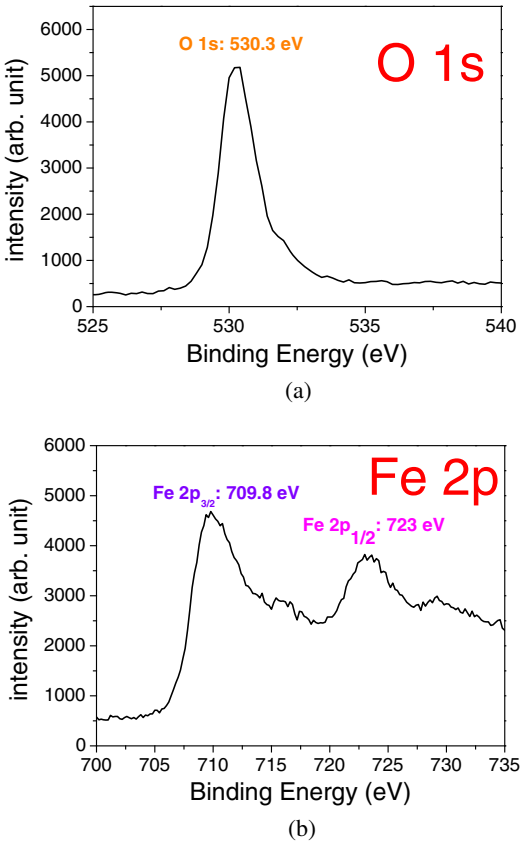

Fig. 7. (Color online) XPS peaks of O 1s (a), Fe 2p (b) for the α-Fe_2O_3 layer.

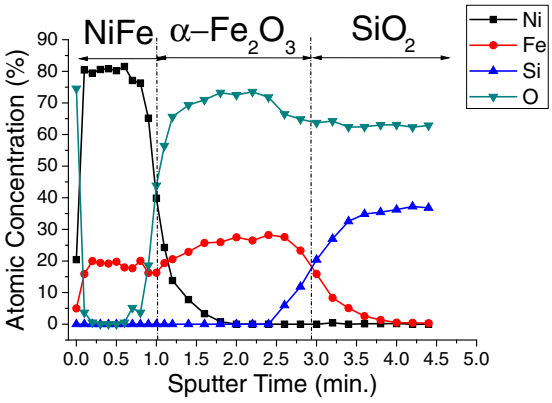

Fig. 8. (Color online) Depth profile analysis of the bombarded [$Ni_{80}Fe_{20}$/α-Fe_2O_3] bilayer.

the intermixing at the $Ni_{80}Fe_{20}/\alpha$-Fe_2O_3 interface was relatively minor, while that at the α-Fe_2O_3/SiO_2 interface was more prevalent.

3.2 Magnetic properties

Figures 9(a)–9(c) show the magnetic hysteresis loops of the un-bombarded bilayer measured at 298, 160, and 10 K, respectively. Figure 9(a) shows a small coercivity of ~2 Oe and no exchange bias for the bilayer with $V_{EH} = 0$ V. These features are similar to those for the pure $Ni_{80}Fe_{20}$ layer.[25–27] The coercivity increased from 2 to 29 Oe as the temperature decreased from 298 to 160 K, due to the decreased thermal energy resulting in a larger field energy being required to rotate the domains in the $Ni_{80}Fe_{20}$. The exchange bias field was still not observed, which could be attributed to the small α-Fe_2O_3 grains that effectively suppressed the Morin transition.[13,21] Figure 9(c) exhibits a pronounced negative exchange bias field (~−260 Oe) and a dramatically enhanced coercivity (~200 Oe). These features can be explained by the reorganization of the antiferromagnetic ordering below the Morin temperature, which is below 100 K in this case.[13] This spin-flop transition permitted a full antiferromagnetic structure that enabled a unidirectional anisotropy so that the exchange coupling between the $Ni_{80}Fe_{20}$ and α-Fe_2O_3 layer led to a large coercivity and exchange bias field.

Figures 10(a)–10(c) present the hysteresis loops of the bombarded bilayer measured at 298, 160, and 10 K, respectively. Figure 10(a) shows a slightly rounded hysteresis loop for the bombarded bilayer at room temperature, indicating a slight offset for the $Ni_{80}Fe_{20}$ easy-axis after the bombardment. In contrast to the room-temperature behaviour, the *M*–*H* loop retained a square shape at both 160 and 10 K, as shown in Figs. 10(b) and 10(c).

The temperature dependence of the coercivity (H_c) and exchange bias field (H_{ex}) for the bilayers without and with bombardment is shown in Fig. 11. The coercivity exhibited a distinct reduction after the ion-beam bombardment, implying that the uniaxial anisotropy in the ferromagnetic layer was dramatically reduced.[28] Such a reduction in uniaxial anisotropy was likely attributed to the irreversible transition in the α-Fe_2O_3 grains caused by the bombardment,[29] which subsequently modified the anisotropy in the $Ni_{80}Fe_{20}$ layer. The exchange bias field however remained

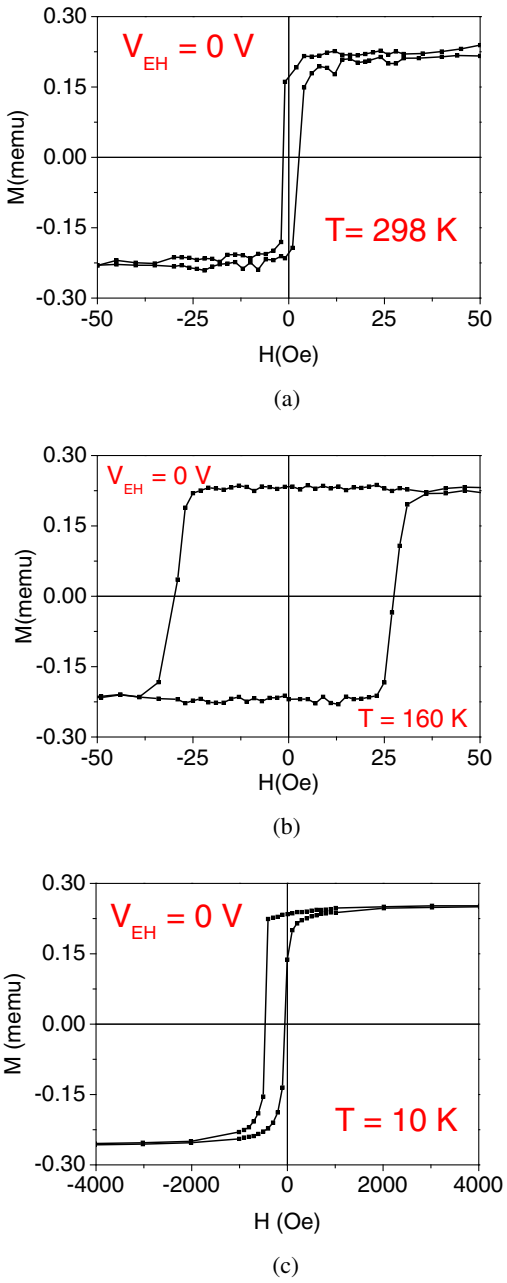

Fig. 9. (Color online) Magnetic hysteresis loops of the un-bombarded [$Ni_{80}Fe_{20}/\alpha$-Fe_2O_3] bilayer measured at 298 (a), 160 (b), and 10 K (c), respectively.

almost the same, implying an unchanged unidirectional anisotropy in the bilayers. These results are consistent with the fact that the coercivity and exchange bias effect are of different origins.[30,31]

To further investigate the nature of exchange coupling in both types of the bilayers, we measured the temperature dependence of the ZFC and FC DC low field (100 Oe) susceptibility, shown in Fig. 12. The magnetization values for the un-bombarded and bombarded bilayers were normalized by their corresponding magnetizations with FC at 10 K. The FC magnetization gradually increased with the decreasing temperature, whereas the ZFC magnetization presented a decrease below ~100 K for both bombarded and un-bombarded bilayers, indicating that the crystallites were no longer superparamagnetic below ~100 K, i.e., their blocking

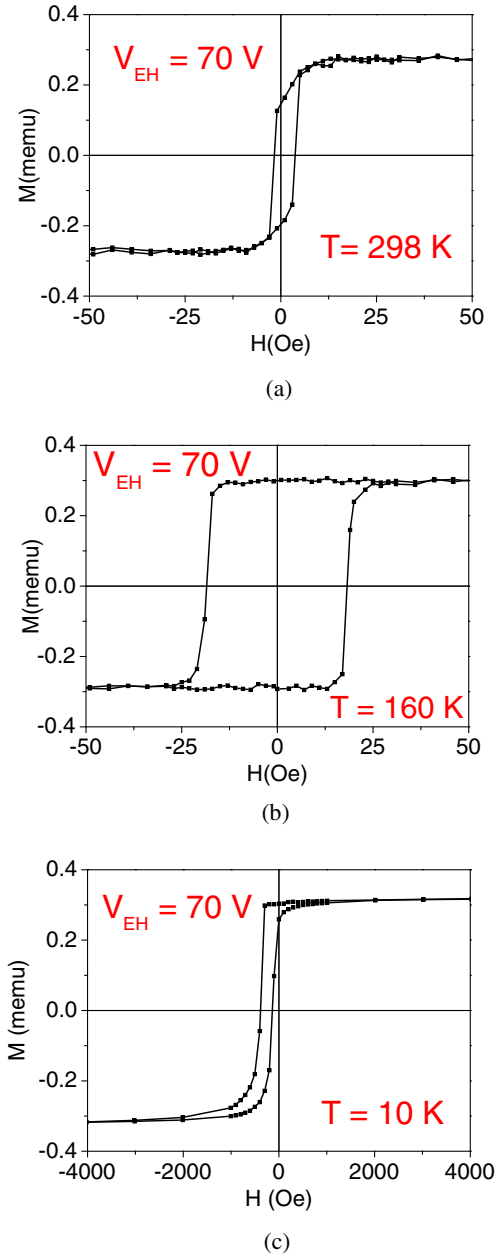

Fig. 10. (Color online) Magnetic hysteresis loops of the bombarded [$Ni_{80}Fe_{20}/\alpha$-Fe_2O_3] bilayer measured at 298 (a), 160 (b), and 10 K (c), respectively.

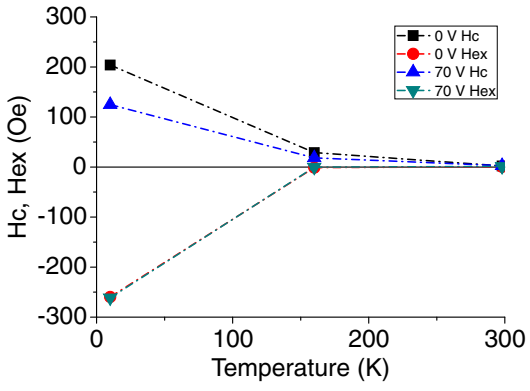

Fig. 11. (Color online) Temperature dependence of the coercivity (H_c) and exchange bias field (H_{ex}) for the un-bombarded and bombarded [$Ni_{80}Fe_{20}/\alpha$-Fe_2O_3] bilayers.

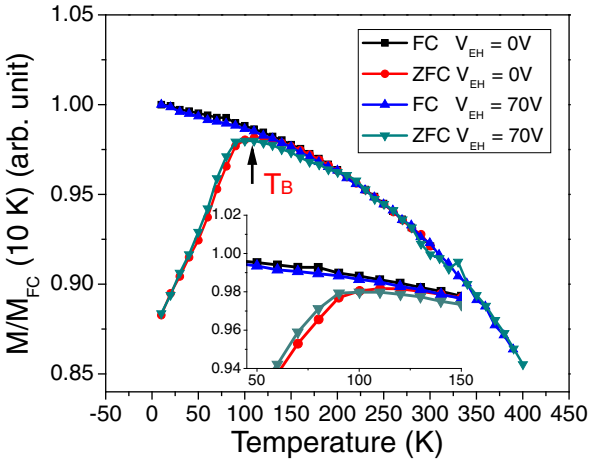

Fig. 12. (Color online) Temperature dependence of the ZFC and FC DC susceptibility for the un-bombarded and bombarded [$Ni_{80}Fe_{20}/\alpha$-Fe_2O_3] bilayers. The magnetization values for the un-bombarded and bombarded [$Ni_{80}Fe_{20}/\alpha$-Fe_2O_3] bilayers were normalized by their corresponding magnetizations with FC at 10 K. The inset shows the ZFC and FC DC susceptibility with the temperature varying from 40 to 150 K.

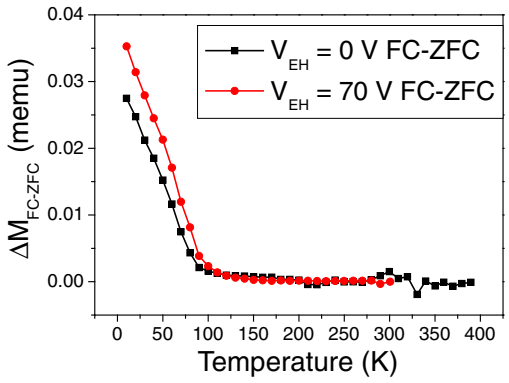

Fig. 13. (Color online) Temperature dependence of the ΔM_{FC-ZFC} for the un-bombarded and bombarded [$Ni_{80}Fe_{20}/\alpha$-Fe_2O_3] bilayer.

temperature (T_B) where the thermal energy was low enough to permit the onset of exchange coupling was around 100 K. These features also indicate that the intrinsic exchange coupling energy between interfaces was unaltered by the interfacial roughness, implying that the similar compositional interface intermixing was occurring in both bilayer systems that was the dominant mechanism for the ferromagnetic/antiferromagnetic exchange coupling. The influence of the ion-beam bombardment on the degree of divergence (ΔM_{FC-ZFC}) was also studied. As shown in Fig. 13, a larger ΔM_{FC-ZFC} below 100 K was observed in the bombarded sample. This can be attributed to the bombardment effect that increased the uncompensated spins at the $Ni_{80}Fe_{20}/\alpha$-Fe_2O_3 interface, resulting in a larger interfacial (canted) magnetization (i.e., larger ΔM_{FC-ZFC}).

4. Conclusions

We carried out a systematic experimental study on the microstructure and magnetic properties of polycrystalline $Ni_{80}Fe_{20}/\alpha$-Fe_2O_3 bilayers with ion-beam bombardment. The low-energy bombardment led to a decline of crystallinity, which was attributed to the increased interfacial defects

induced by the bombardment. After the ion-beam bombardment, the coercivity exhibited a distinct reduction, implying that the uniaxial anisotropy in the ferromagnetic layer was dramatically reduced. The almost identical blocking temperatures for the un-bombarded and bombarded bilayers indicate that the intrinsic exchange coupling energy between interfaces was unaltered by the interfacial roughness, implying that the similar compositional interface intermixing was occurring in both bilayer systems that was the dominant mechanism for the ferromagnetic/antiferromagnetic exchange coupling. A larger ΔM_{FC-ZFC} was observed in the bombarded bilayer which was a result of the additional uncompensated spins created by the bombardment effect at the $Ni_{80}Fe_{20}/\alpha$-Fe_2O_3 interface. These uncompensated spins resulted in a stronger exchange coupling, which possibly in turn reduced the relative twisting in the $Ni_{80}Fe_{20}$ layer and thus gave rise to a smaller coercivity. In order to fully explain the phenomena observed here, a theoretical study that considers the effect of finite grain-size and temperature-varying anisotropy in addition to the magnetic properties already known for bulk α-Fe_2O_3 needs to be conducted in the future.

Acknowledgments

This work was supported in part by NSC of Taiwan, NSERC and CFI Programs of Canada, and the Seed Funding Program for Basic Research and Small Project Funding Program from the University of Hong Kong, ITF Tier 3 funding (ITS/104/13), RGC-GRF grant (HKU 704911P), and University Grants Committee of Hong Kong (Contract No. AoE/P-04/08).

1) K. Brezesinski, J. Haetge, J. Wang, S. Mascotto, C. Reitz, A. Rein, S. H. Tolbert, J. Perlich, B. Dunn, and T. Brezesinski, Small **7**, 407 (2011).
2) Y. Ren, Z. Ma, and P. G. Bruce, CrystEngComm **13**, 6955 (2011).
3) J. K. Oh and J. M. Park, Prog. Polym. Sci. **36**, 168 (2011).
4) B. Koo, H. Xiong, M. D. Slater, V. B. Prakapenka, M. Balasubramanian, P. Podsiadlo, C. S. Johnson, T. Rajh, and E. V. Shevchenko, Nano Lett. **12**, 2429 (2012).
5) W.-C. Lin, H.-Y. Chang, Y.-T. Hu, and C.-C. Kuo, Jpn. J. Appl. Phys. **48**, 08JB07 (2009).
6) J. I. Fujita, M. Ishida, T. Ichihashi, Y. Ochiai, T. Kaito, and S. Matsui, Jpn. J. Appl. Phys. **43**, 3799 (2004).
7) M. Mahmoudi, A. S. Milani, and P. Stroeve, Int. J. Biomed. Nanosci. Nanotechnol. **1**, 164 (2010).
8) M. Mahmoudi, A. Simchi, M. Imani, and U. O. Hafeli, J. Phys. Chem. C **113**, 8124 (2009).
9) S. Chatterjee, A. Bandyopadhyay, and K. Sarkar, J. Nanobiotechnol. **9**, 34 (2011).
10) M. Blanchard, M. Lazzeri, F. Mauri, and E. Balan, Am. Mineral. **93**, 1019 (2008).
11) R. Winpenny, *Molecular Cluster Magnets* (World Scientific, Singapore, 2012) Vol. 3.
12) H. S. Nabi, R. J. Harrison, and R. Pentcheva, Phys. Rev. B **81**, 214432 (2010).
13) D. L. Cortie, K. W. Lin, C. Shueh, H. F. Hsu, X. L. Wang, M. James, H. Fritzsche, S. Brück, and F. Klose, Phys. Rev. B **86**, 054408 (2012).
14) R. D. Zysler, D. Fiorani, A. M. Testa, L. Suber, E. Agostinelli, and M. Godinho, Phys. Rev. B **68**, 212408 (2003).
15) R. Xu, H. Yan, W. Y. He, Y. Su, J. C. Nie, and L. He, J. Phys. Chem. C **116**, 6879 (2012).
16) S. Park, H. Jang, J. Y. Kim, B. G. Park, T. Y. Koo, and J. H. Park, Europhys. Lett. **103**, 27007 (2013).
17) J. Nogués and I. K. Schuller, J. Magn. Magn. Mater. **192**, 203 (1999).
18) F. Zhou, B. Yue, X. Wang, X. Wu, and L. Zhuge, J. Alloys Compd. **492**, 269 (2010).
19) S. Nakashima, Y. Takada, S. Seto, H. Fujisawa, O. Sakata, Y. Katsuya, M. Kobune, and M. Shimizu, Jpn. J. Appl. Phys. **52**, 09KB03 (2013).
20) G. Nahrwold, J. M. Scholtyssek, S. Motl-Ziegler, O. Albrecht, U. Merkt, and G. Meier, J. Appl. Phys. **108**, 013907 (2010).
21) R. N. Bhowmik and A. Saravanan, J. Appl. Phys. **107**, 053916 (2010).
22) G. Li, C. W. Leung, C. Shueh, H.-F. Hsu, H.-R. Huang, K.-W. Lin, P. T. Lai, and P. W. T. Pong, Surf. Coatings Technol. **228**, S437 (2013).
23) C. Wagner, in *Handbook of X-ray Photoelectron Spectroscopy*, ed. G. E. Muilenberg (Perkin-Elmer, Eden Prairie, MN, 1979) p. 80.
24) N. S. McIntyre and D. G. Zetaruk, Anal. Chem. **49**, 1521 (1977).
25) C. Nistor, E. Faraggi, and J. L. Erskine, Phys. Rev. B **72**, 014404 (2005).
26) A. V. Svalov, I. R. Aseguinolaza, A. Garcia-Arribas, I. Orue, J. M. Barandiaran, J. Alonso, M. L. Fernández-Gubieda, and G. V. Kurlyandskaya, IEEE Trans. Magn. **46**, 333 (2010).
27) K. W. Lin and J. Y. Guo, J. Appl. Phys. **104**, 123913 (2008).
28) C. Shueh, P. S. Chen, D. Cortie, F. Klose, W. C. Chen, T. H. Wu, J. Van Lierop, and K. W. Lin, Jpn. J. Appl. Phys. **51**, 11PG02 (2012).
29) M. D. Stiles and R. D. McMichael, Phys. Rev. B **63**, 064405 (2001).
30) G. Scholten, K. D. Usadel, and U. Nowak, Phys. Rev. B **71**, 064413 (2005).
31) C. Leighton, H. Suhl, M. J. Pechan, R. Compton, J. Nogues, and I. K. Schuller, J. Appl. Phys. **92**, 1483 (2002).